Thermal expansion of a La-based bulk metallic glass: insight from in-situ high-energy X-ray diffraction

J Bednarcik[1]‡, S Michalik[1,2], M Sikorski[1,3], C Curfs[4], XD Wang[5], JZ Jiang[5] and H Franz[1]

[1] Deutsches Elektronen-Synchrotron DESY, Notkestrasse 85, D-22603 Hamburg, Germany

[2] Institute of Physics, Faculty of Science, P.J. Šafárik University, Park Angelinum 9, 041 54 Košice, Slovakia

[3] Advanced Photon Source, Argonne National Laboratory, Argonne, Illinois 60439, USA

[4] European Synchrotron Radiation Facility ESRF, BP 220, 38043 Grenoble, France

[5] International Center for New-Structured Materials ICNSM, Zhejiang University and Laboratory of New-Structured Materials, Department of Materials Science and Engineering, Zhejiang University, Hangzhou 310027, P.R. China

E-mail: `jozef.bednarcik@desy.de`

Abstract. Constant-rate heating experiments using a fast x-ray camera (time resolution of 2.7 s) reveal detailed information about the thermal stability of $La_{62}Al_{14}(Cu_{5/6}Ag_{1/6})_{14}Ni_5Co_5$ (at.%) bulk metallic glass. Analyzing diffraction patterns in reciprocal space yields the thermal expansion of the amorphous alloy providing insight about the thermally activated relaxation effects and kinetics of the glass transition. The glass transition appears as a break in the value of the coefficient of volume thermal expansion. Furthermore, real space analysis based on reduced pair distribution function $G(r)$ allows one to follow in-situ the changes in the local atomic structure of the amorphous material during constant-rate heating.

PACS numbers: 61.05.cp, 61.43.Dq, 65.60.+a, 64.70.pe

Submitted to: *J. Phys.: Condens. Matter*

‡ Author to whom any correspondence should be addressed

1. Introduction

Recently, after the discovery of several families of multi-component alloys exhibiting a large supercooled liquid region before crystallization [1], bulk metallic glass (BMG) formation has become a common phenomenon. Samples with dimensions in the cm range have been prepared by simple mould casting with a cooling rate lower than 100 K/s. For example, a maximum diameter of cast cylinders of about 72 mm for $Pd_{40}Cu_{30}Ni_{10}P_{20}$ [2], 25 mm for $Mg_{54}Cu_{26.5}Ag_{8.5}Gd_{11}$ [3], 35 mm for $La_{62}Al_{14}(Cu_{5/6}Ag_{1/6})_{14}Ni_5Co_5$ [4] and more than 20 mm for $Zr_{46}(Cu_{4.5/5.5}Ag_{1/5.5})_{46}Al_8$ [5] were achieved.

High-energy X-ray diffraction (XRD) has proven to be a suitable tool to determine the local atomic structure of the metallic glasses [6]. Time-resolved in-situ XRD experiments performed at high-brilliance synchrotron radiation sources can detect tiny changes of the amorphous structure when exposed to a variety of temperature-pressure conditions [7, 8]. It was recently demonstrated that high-energy X-ray scattering can be used to measure the elastic strain under compression [9, 10] and tension [11, 12] and to detect the change in excess free volume upon heating [13].

In this work we present a study of the volume expansion occurring upon heating/cooling of a $La_{62}Al_{14}(Cu_{5/6}Ag_{1/6})_{14}Ni_5Co_5$ (at.%) BMG based on inverse and real space analysis using in-situ high-energy XRD. Special emphasis is placed on the better understanding of thermally activated relaxation and the glass transition.

2. Experimental techniques

2.1. Sample preparation

Copper mould casting was used to prepare bulk metallic glasses with nominal composition $La_{62}Al_{14}(Cu_{5/6}Ag_{1/6})_{14}Ni_5Co_5$ (at.%). Sample preparations started with Cu-Ag-Ni-Co ingots which were then arc-melted together with La and Al to obtain the final composition. The purities of the elements ranged from 99.5 to 99.98 at.%. The ingots were remelted at least four times to achieve chemical homogeneity. The master alloys were further processed by suction-casting into copper mold (with diameter of 0.9 mm) under a purified argon atmosphere. The obtained rods were cut into 5 mm long pieces which were used for further investigations.

2.2. Calorimetric and dilatometric measurements

A differential scanning calorimeter (Netzsch DSC 404C) was used to detect the crystallization and melting behavior of the as-prepared BMG under a continuous argon flow at a heating rate of 20 K/min. The thermal expansion was investigated by a Netzsch DIL 402 C dilatometer (heating rate 5 K/min).

2.3. "Slow" in-situ x-ray scattering experiments

The amorphous nature and the temperature stability of the as-cast sample was verified by using high-energy X-ray diffraction (XRD) at the BW5 wiggler beamline at the positron storage ring DORIS at DESY/HASYLAB (Hamburg, Germany). The beam size was 0.25×0.25 mm^2 and the wavelength of 0.124 Å (photon energy 100 keV) was selected using a gradient Si/Ge(111) monochromator. XRD patterns were collected in transmission mode using a MAR345 two-dimensional (2D) image plate detector (3450×3450 pixels, 100×100 μm^2 pixel size) providing a sufficient range in the modulus of the scattering vector ($q = 4\pi sin(\theta)/\lambda$) of 16 Å^{-1}. 1 mm thick aluminium sheet was placed just in front of two-dimensional detector in order to suppress background. Rod shaped samples with typical diameter and length of 0.9 and 5 mm respectively, were sealed in thin-walled quartz capillaries. The samples were annealed in a temperature range of 330-440 K with steps of 5 K in a vacuum better than 10^{-2} Pa (10^{-4} mbar) using a mirror furnace utilizing two infrared lamps. After reaching the desired temperature samples were illuminated for 30 s and 2D diffraction data were recorded. Due to the relatively long readout time of the MAR345 (about 100 s), write-to-disc time and temperature stabilization the total temporal resolution was about 200 s and thus yielding an average heating/cooling rate of 1.5 K/min.

2.4. "Fast" in-situ x-ray scattering experiments

The temperature evolution of the as-cast rods was continuously followed in-situ using the high-energy monochromatic beam on the ID11 undulator beamline at ESRF (Grenoble, France). Again rod shaped samples having diameter of 0.9 mm and length of 4 mm were sealed in thin-walled quartz capillaries. Annealing was done in Ar-protective atmosphere using a Linkam THMS 600. The wavelength of $\lambda = 0.1409$ Å (photon energy 88 keV) was selected using a Si(111) monochromator. XRD patterns were collected in transmission mode using a fast two-dimensional CCD detector FRELON 2k16 (2048×2048 pixels, 50×50 μm^2 pixel size). The delay between consecutive patterns, due to read-out time of the CCD and write-time to hard-disc was 2.7 s. Two-dimensional XRD patterns were integrated using the FIT2D software package [14]. Series of XRD patterns were acquired during constant-rate heating from room temperature up to 773 K, well above the melting point of the alloy. In total six independent in-situ experiments were performed using different heating rates Φ (2, 5, 10, 20, 50 and 100 K/min). Furthermore this setup was used to determine part of the Temperature-Time-Transformation (TTT) diagram of the investigated alloy.

3. Theoretical background

3.1. Structure factor and pair distribution function

The total structure factor, $S(q)$, was obtained using standard procedures described in [6, 15]. The integrated intensity distributions $I(q)$ were corrected by considering

background, sample absorption, fluorescence contribution and inelastic (Compton) scattering [16]. Absorption of the sample at a given energy was determined by measuring incoming and transmitted beam intensity using beam monitor diode. To suppress fluorescence background we put 1 mm thick aluminium sheet on the front face of 2D detector. To place data on an absolute scale, we employed high-angle region method [15]. Further we assumed isotropic fluorescence intensity which was adjusted to a constant value based on the behavior of the resulting structure factor $S(q)$. Once selected, the same fluorescence intensity was used for all the data sets.

The total structure factor $S(q)$ was obtained from the normalized elastically scattered intensity, $I_e(q)$ using the Faber-Ziman formalism [17]

$$S(q) = 1 + \frac{I_e(q) + \left[\sum_{i=1}^{N} c_i f_i^2(q)\right]}{\left[\sum_{i=1}^{N} c_i f_i(q)\right]^2}, \tag{1}$$

where c_i and $f_i(q)$ are the atomic concentration and the x-ray scattering factor of the atomic species of type i (i = La, Al, Cu, Ag, Ni, Co), respectively. The corresponding reduced pair distribution function, $G(r)$, can be obtained through a sine Fourier transformation

$$G(r) = 4\pi r[\rho(r) - \rho_0] = \frac{2}{\pi}\int_0^\infty q\,[S(q) - 1]\sin(rq)dq, \tag{2}$$

where $\rho(r)$ and ρ_0 are the local and average atomic number densities, respectively, and r is the radial distance. Since $\rho(r)$ becomes zero below a certain r_{min}, the average atomic number density ρ_0 can be easily obtained by linear fit of $G(r)$'s low part (where $r \leq r_{min}$) to $-4\pi\rho_0 r$. From $G(r)$ the radial distribution function, $RDF(r)$, can be calculated by

$$RDF(r) = 4\pi r^2\rho(r) = 4\pi r^2\rho_0 + rG(r). \tag{3}$$

The average coordination number, N, around any given atom in a spherical shell between radius r_1 and r_2 can be calculated as

$$N = \int_{r_1}^{r_2} RDF(r)dr. \tag{4}$$

3.2. Thermal expansion from X-ray scattering

As proposed by Yavari and co-workers [13] the third power of the principal peak position Q scales with the coefficient of volume thermal expansion α_{th} of isotropic amorphous solid as in

$$\left\{\frac{Q(T_0)}{Q(T)}\right\}^3 = \frac{V(T)}{V(T_0)} = 1 + \alpha_{th}(T - T_0), \tag{5}$$

where $V(T)/V(T_0)$ is the reduced mean atomic volume at temperature T, with the reference temperature T_0 (in our study 330 K). It should be noted here that for isotropic materials, the linear thermal expansion coefficient β_{th} is one third the volumetric

coefficient α_{th}, i.e. $\alpha_{th} = 3\beta_{th}$. Yavari and co-workers [13] used Equation (5) to quantify the free volume changes in a $Pd_{40}Ni_{30}Cu_{10}P_{20}$ metallic glass associated with the thermally activated relaxation. Hufnagel and co-workers [10] have used a similar concept to determine the strain of elastically deformed bulk amorphous $Zr_{57}Ti_5Cu_{20}Ni_8Al_{10}$ from the relative changes of principal peak position Q.

To obtain quantitative results about the thermal expansion form X-ray diffraction data the profile of the first (principal) diffraction peak was modelled assuming a linear background and a pseudo-Voigt function $I_P(q)$ having the analytical form

$$I_P(x) = A\left[\gamma C(x) + (1-\gamma)G(x)\right], \tag{6}$$

where A is the amplitude, $C(x) = (1+x^2)^{-1}$ represents the Cauchy and $G(x) = \exp[-(\ln 2)x^2]$ the Gaussian part, with $x = (q-Q)/w$, in which $2w$ is the full-width at half-maximum (FWHM), γ the Cauchy content and Q the position of the peak maximum. The peak position Q and other profile parameters were determined by nonlinear least-squares fit of the pseudo-Voigt function to a set of data points corresponding to the principal diffraction peak. Since more data points are considered for determining the peak position, the influence of the error of an individual data point on the peak position is minimized. As can be seen from the inset in Figure 1a, the pseudo-Voigt function satisfactorily describes the shape of the principal peak.

In principle one should first convert all measured intensities $I(q)$ into corresponding structure functions $S(q)$ and then use those for tracing the position of the principal peak. We actually tested both $I(q)$ and $S(q)$ datasets. We found that the thermal expansion curves obtained are equal for both approaches, indicating that the q dependence of the $\langle f(q)\rangle^2$ in Equation (1) is not significant for the small peak shifts that occur due to thermal loading. Similar conclusions were reported in [10].

4. Results and discussion

4.1. Thermal cycling and relaxation phenomena

A room temperature XRD pattern of a rod-shaped $La_{62}Al_{14}(Cu_{5/6}Ag_{1/6})_{14}Ni_5Co_5$ sample in the as-cast state is shown in Figure 1a. The intensity curve $I(q)$ shows a pronounced diffuse peak located at $q = 2.19$ Å^{-1} and rather broad and sharply decaying oscillations which are almost buried in noise above 12 Å^{-1}. Such a pattern is a fingerprint of the missing long-range order and confirms the fully amorphous nature of the as-casted material. Figure 1b shows the structure factor $S(q)$ calculated from the corresponding $I(q)$ (shown in Figure 1). The thermal cycling in the temperature range between 330 and 440 K at 1.5 K/min yielded a series of similar XRD patterns.

Figure 2 shows the relative volume changes for an as-cast rod as observed by in-situ XRD during thermal cycling between 330 and 440 K at 1.5 K/min. It is seen that during the first heating run the initial volume changes are positive while an opposite behavior is observed after reaching the temperature of 378±5 K (we refer to as relaxation temperature T_r). A negative volume change follows until reaching a second characteristic

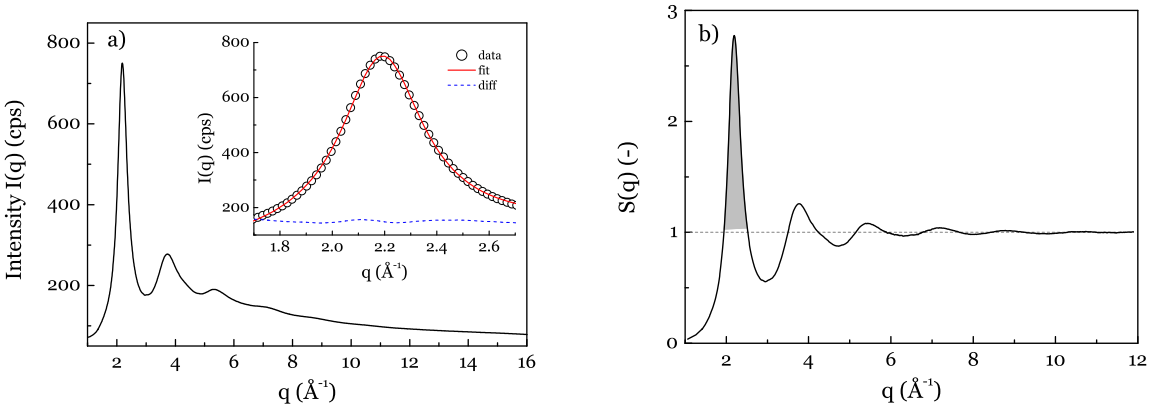

Figure 1. (Color online) a) Room temperature XRD pattern of a $La_{62}Al_{14}(Cu_{5/6}Ag_{1/6})_{14}Ni_5Co_5$ rod in the as-cast state. The inset shows the principal peak fitted with a pseudo-Voigt function given by Equation (6). b) Structure factor $S(q)$ calculated from the pattern $I(q)$ shown in a). The shading depicts the region of the principal peak which was modelled using the pseudo-Voigt profile.

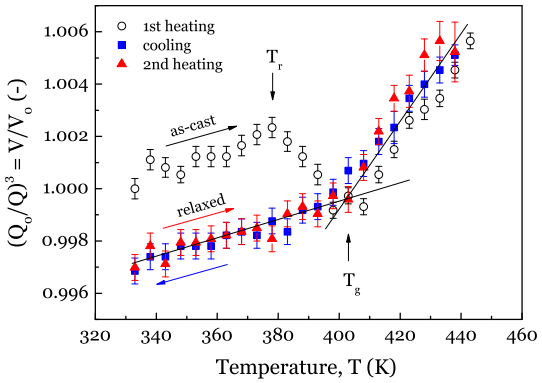

Figure 2. (Color online) Relative volume changes for an as-cast rod as observed by in-situ XRD during thermal cycling between 330 and 440 K at 1.5 K/min. Arrows indicate the onset of relaxation T_r and glass transition T_g temperature.

temperature when an abrupt change of the slope is observed. This point we identify as the glass transition temperature T_g=403±5 K. The coefficient of volume thermal expansion α_{th} between T_0 and T_r reaches a value of $(4.2 \pm 0.8) \times 10^{-5}$ K^{-1} while above T_g it is about three times larger $(13.0 \pm 0.9) \times 10^{-5}$ K^{-1}. The anomalous decrease of the volume between T_r and T_g can be explained in terms of structural relaxation. The amorphous structure in this temperature range relaxes by annealing structural defects which are introduced during casting of the bulk sample [18, 19]. Similar results, however on different metallic glasses, were reported in [20]. When cooling from 420 K down to the glass temperature T_g the relative volume changes are reversible. Further cooling from T_g down to T_0 shows a significant deviation from the first heating run indicating

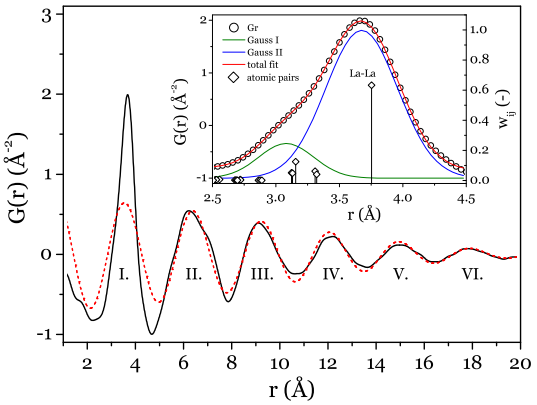

Figure 3. (Color online) Reduced pair distribution function $G(r)$ (full line) calculated from structure function $S(q)$ shown in Fig.1b using Equation (2). Roman numerals denote respective coordination shells. The red dashed line represents the result of the sine Fourier transformation of the principal peak (see shaded peak in Fig.1b) appearing in $S(q)$ and covering a q-range $\langle 1.94, 2.52\rangle$ Å^{-1}. The inset shows a detailed view of the first coordination sphere together with interatomic bond lengths (calculated as sum of the atomic radii) and corresponding X-ray scattering weights w_{ij}. Furthermore, the full lines represent the decomposition of the first shell into two Gaussians.

that irreversible structural changes happened during the initial heating run. On the other hand the second heating run matches the cooling curve completely within the experimental uncertainty and reveals no hysteresis.

So far we discussed the thermal expansion behavior based on reciprocal space analysis. In order to follow these changes in real space, the diffracted intensity distributions $I(q)$ were converted to the corresponding structure functions $S(q)$ according Equation (1) which were subsequently Fourier transformed using Equation (2) yielding the corresponding reduced pair distribution functions $G(r)$. Figure 3 shows the reduced pair distribution function (PDF) $G(r)$ at room temperature obtained by sine Fourier transform (FT) of the structure function $S(q)$ (shown in Figure 1b) on the full q-range $\langle 0, 12\rangle$ Å^{-1} . It is interesting to observe what happens to the pair distribution function if we perform the FT with limited q-range $\langle 1.94, 2.52\rangle$ Å^{-1}, covering the principal peak only. In this way we obtain a modified pair distribution function (see red dashed line in Figure 3a) whose tail perfectly matches the complete $G(r)$ above 11 Å. This suggests that thermal expansion determination based on reciprocal space analysis (tracing of the principal peak position in diffracted intensities $I(q)$) is more sensitive to medium or more to long range interatomic correlations. In other words reciprocal space analysis gives good agreement with macroscopic observation of thermal expansion. This is consistent with other observations which showed that tracing of the principal peak in reciprocal space yields basically the same expansion curve (at least up to T_g) as conventional macroscopic dilatometry measurements [13]. Further one can readily see that the sine FT of the principal peak poorly reproduces the short range

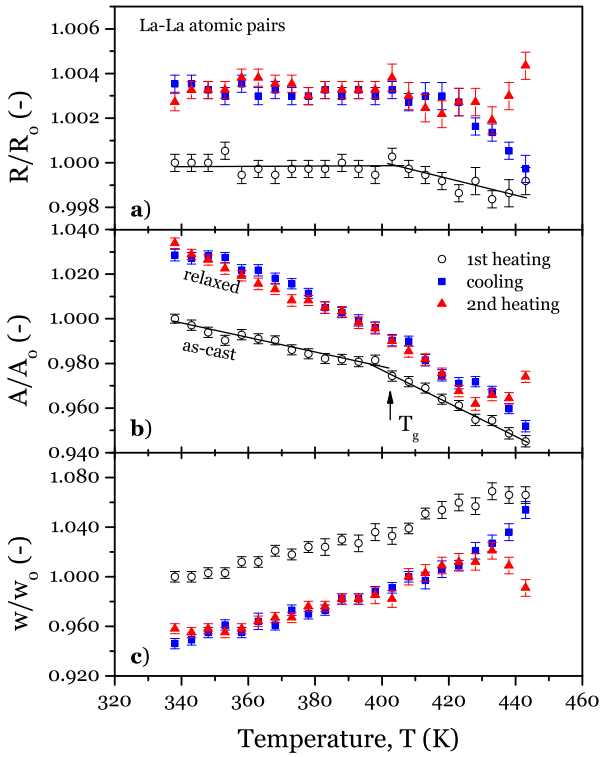

Figure 4. (Color online) Relative change of the profile parameters (peak position R, amplitude A and width w) of the Gaussian describing the distribution of La-La interatomic bond lengths in the first coordination sphere during thermal cycling between 330 and 440 K at 1.5 K/min.

interatomic correlations. In order to observe fine structural alterations occurring in the nearest atomic neighborhood it is inevitable to perform the sine FT on a q-range as wide as possible.

For the $La_{62}Al_{14}(Cu_{5/6}Ag_{1/6})_{14}Ni_5Co_5$ glass, there are 21 possible nearest-neighbour partials with corresponding X-ray weights w_{ij}. However, from the type and concentration of the constituent elements in the alloy it is evident that the La-La atomic pairs are the ones which determine the shape of the first broad maximum in $G(r)$ (range 2.5-4.5 Å). Its asymmetric shape results from the weak contribution of La-M type (M=Al,Cu,Ag,Ni,Co) atomic pairs in the range between 2.5 and 3.5 Å. The inset in Figure 3 shows a decomposition of the first broad maximum appearing in $G(r)$ into two Gaussians together with the interatomic bond lengths (sum of atomic radii) and the corresponding weight factors w_{ij} (denoted by open diamonds).

Figure 4 shows the evolution of the relative changes of the profile parameters (with respect to $T_0 = 330$ K) such as peak position R, amplitude A and half-width at half-maximum w of the Gaussian describing the contribution of La-La atomic pairs to the first coordination shell. As can be seen from Figure 4a, the first heating run up to T_g has no substantial influence on the relative peak position R/R_0. However, after reaching T_g it tends to decrease and reduces its value by 0.1%. When cooling back to 330 K,

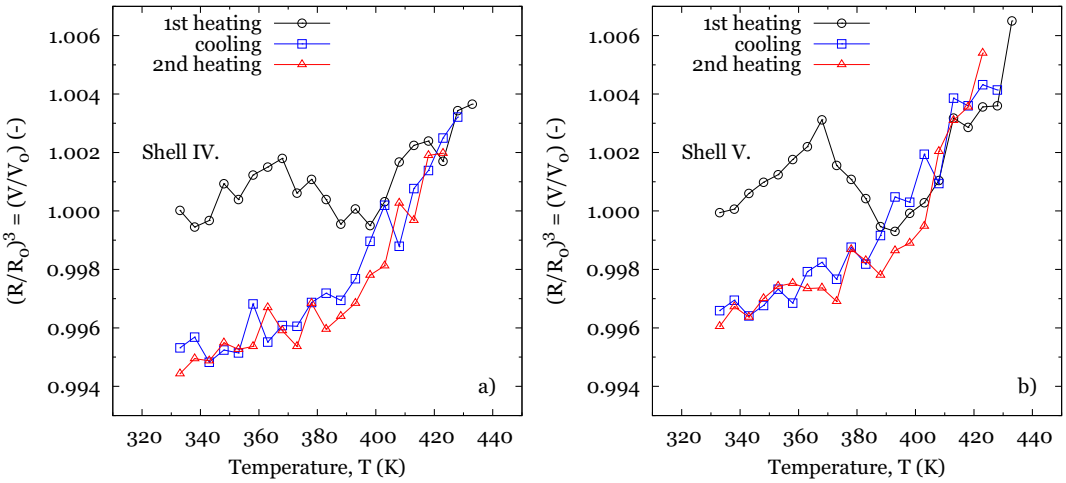

Figure 5. (Color online) Relative change of the center of mass of the a) coordination shell IV. with r-range $\langle 11.5, 12.9 \rangle$ Å and b) coordination shell V. with r-range $\langle 14.3, 15.8 \rangle$ Å during thermal cycling between 330 and 440 K at 1.5 K/min. Corresponding coordination shells are depicted in Figure 3.

the value of R/R_0 gradually increases and below T_g saturates at 0.3±0.05 % above the initial value of R_0 (3.676 Å at $T_0 = 330$ K). The second heating run basically coincides with the cooling part. The temperature evolution of the relative peak amplitude A/A_0 (Figure 4b) and the relative peak width w/w_0 (Figure 4c) reveals a much higher effect of annealing as compared to the temperature dependence of R/R_0. After cooling the peak amplitude A increased by 3 % whereas the peak width w decreased by almost 6 %.

In-situ XRD experiments performed on a $Cu_{55}Hf_{25}Ti_{15}Pd_5$ BMG showed that the thermal expansion coefficient value of the glassy solid determined by the shift of the x-ray diffraction maximum (in reciprocal space) or PDF maximum (in real space) give good agreement [21]. Similar conclusions were drawn from thermal expansion data obtained on $Ge_{50}Al_{40}Cr_{10}$ amorphous alloy [22]. Contrary, our current measurements on $La_{62}Al_{14}(Cu_{5/6}Ag_{1/6})_{14}Ni_5Co_5$ BMG show completely different expansion curves when comparing the analysis from reciprocal (see Figure 2) and real (see Figure 4a) space.

Further we were interested what would be the difference when observing thermal response from more distant coordination shells. Figure 5 shows the relative change of the center of mass of the coordination shells IV. and V. (shells are depicted in Figure 3). Relatively good match between thermal expansion data obtained from reciprocal (see Figure 2) and real (see Figure 5) space can be observed. Again this suggests that thermal expansion based on reciprocal space analysis is more sensitive to long range interatomic correlations. Concluding all results described above one may state that reciprocal space analysis based on the principal peak position and real space analysis based on center of the mass of the first coordination shell give in general different results since they are preferentially sensitive to different correlation lengths. Similar conclusions were made from strain measurements using high-energy X-ray scattering on bulk amorphous

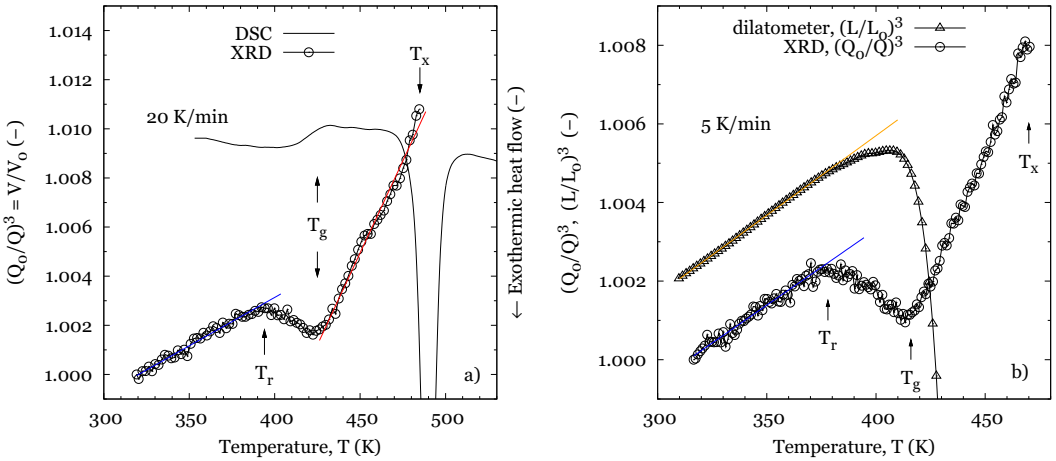

Figure 6. (Color online) a) DSC curve and thermal expansion curve obtained from in-situ XRD measurements performed at a heating rate of 20 K/min. b) Comparison of thermal expansion curves obtained by conventional dilatometry and in-situ XRD measurements performed at a heating rate of 5 K/min. For purposes of better clarity curves are vertically offset. Lines represent a fit to the experimental data using Equation (5). Arrows indicate the onset of the relaxation T_r, glass transition T_g and crystallization T_x temperature.

$Zr_{57}Ti_5Cu_{20}Ni_8Al_{10}$ loaded in uniaxial compression [10]. It was shown that the strain in the nearest-neighbor atomic environment is somewhat smaller than the strain measured over longer length scales.

4.2. Glass transition and kinetics

As can be seen from the DSC curve presented in Figure 6a, the investigated alloy reveals the presence of a relatively wide supercooled liquid region $\Delta T_x = T_x - T_g = 60\,\mathrm{K}$, which starts with the glass temperature $T_g = 422\,\mathrm{K}$ and finishes with the crystallization temperature $T_x = 482\,\mathrm{K}$. The included thermal expansion curve indicate perfect matching of T_g and T_x with the DSC curve. It is interesting to note that DSC measurements reveal almost no hint of the relaxation temperature T_r while the expansion curve shows it expressly. Figure 6b shows a comparison of the thermal expansion curves obtained by conventional dilatometry and in-situ XRD measurements performed at a heating rate of 5 K/min. The initial parts of both expansion curves show within experimental uncertainty the same slope $\alpha_{th} = (3.95 \pm 0.1) \times 10^{-5}\ \mathrm{K}^{-1}$. After reaching T_r the expansion is less pronounced in case of the dilatometry measurements. Our XRD data show even a negative slope above T_r. After reaching the glass temperature T_g the sample significantly softens which prevents further expansion measurements using conventional dilatometry. However, XRD is a contact free method, hence measurements above T_g are possible.

The kinetics of the glass transition of the $La_{62}Al_{14}(Cu_{5/6}Ag_{1/6})_{14}Ni_5Co_5$ bulk metallic glass was investigated by fast in-situ XRD. In total six independent in-situ experiments were performed using different heating rates Φ (2, 5, 10, 20, 50 and 100

K/min). Figure 7 shows the thermal expansion of $La_{62}Al_{14}(Cu_{5/6}Ag_{1/6})_{14}Ni_5Co_5$ BMG at different heating rates as determined from the temperature behaviour of the principal peak position $Q = Q(T)$. Measurements of the thermal expansion at different heating rates reveal three distinct temperature regions (T_0, T_r), (T_r, T_g) and (T_g, T_x), similar to the previous experiments (see Figure 2). However, using a faster detector improves the resolution of the data significantly. The initial increase of the relative volume is connected with the volume thermal expansion of the amorphous phase. Reaching the intermediate maximum around T_r the slope reverts its sign and the relative volume decreases with increasing temperature. Such an anomalous decrease of the volume above T_r can be explained in the terms of relaxation effects. Most probably the amorphous structure in this temperature range relaxes by annealing out structural defects which are introduced when casting the bulk sample. After reaching the glass-transition temperature T_g, a sudden change in the volume expansion coefficient is observed. The further increase of temperature leads to a relatively steep increase of the volume which dramatically drops after reaching the temperature corresponding to the onset of crystallization T_x. Such discontinuity has no physical meaning and indicates that the position of the principal peak has dramatically changed due to superposition with Bragg peaks. Interestingly, all three distinct segments of the expansion curve may be approximated by linear behavior given by Equation (5), which reveals the corresponding coefficient of thermal volume expansion α_{th}. Increasing the heating rate Φ does not influence the coefficient of volume expansion α_{th} between T_0 and T_r and it remains constant at $(3.8 \pm 0.2) \times 10^{-5}$ K^{-1}. This value is rather similar (within the experimental error) to the value determined from the data presented in Figure 2. Similarly the value of α_{th} is about three times larger ($(14.6 \pm 0.3) \times 10^{-5}$ K^{-1}) above T_g than below T_r. Furthermore, the slight dependence of α_{th} on heating rate Φ for the temperature ranges (T_r, T_g) and (T_g, T_x) is mostly due to the increase of noise in our data, specially true for heating rates greater than 20 K/min, when curves with a lower number of scans are acquired. Measurements well above the melting point reveal a linear thermal volume expansion with a positive slope of $\alpha_{th} = (9.9 \pm 0.1) \times 10^{-5}$ K^{-1} which does not depend on heating rate. Thermal cycling in the molten state above the liquidus temperature T_l (708 K @ 2 K/min) confirms that the volume expansion in this temperature range is fully reversible.

In order to observe the thermal expansion behavior on a level of the atomic nearest neighborhood we converted all acquired diffraction patterns to corresponding pair distribution functions. We were further interested to observe the thermal evolution of the La-La interatomic bond length, which is the most dominant correlation length in the first coordination sphere. As can be seen from Figure 8 heating a sample at 2 K/min up to T_r practically does not affect the La-La interatomic bond length. Further increasing temperature causes the La-La bond length to slightly increase. After reaching T_g the La-La bond length reveals a local maximum and tends to decrease with further increasing temperature. Around 450 K the curve changes back to positive slope and steeply rises up to T_x. It is interesting to note that the thermal expansion curve based on

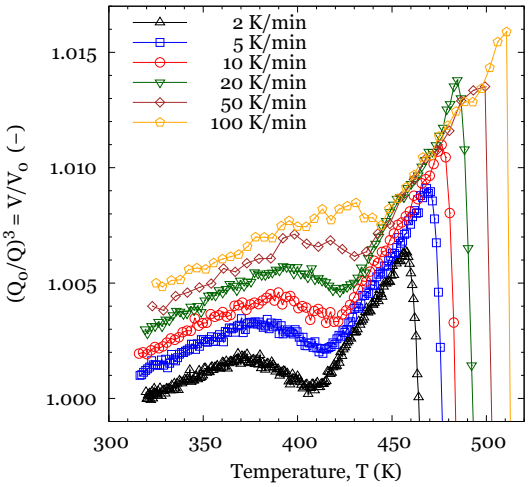

Figure 7. (Color online) Thermal expansion of the amorphous phase as determined from the temperature behavior of the principal peak position traced at different heating rates Φ. For purposes of better clarity all curves are vertically offset by 0.001.

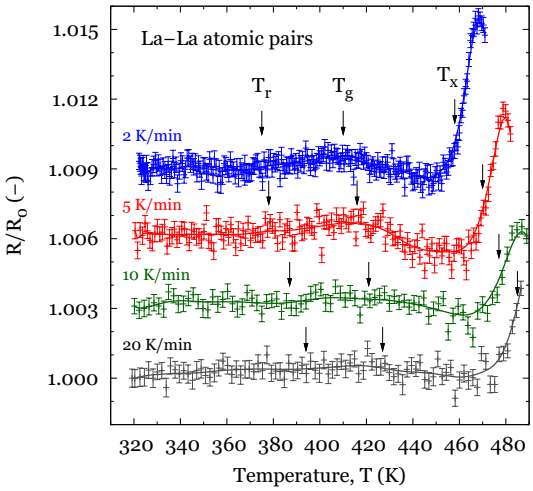

Figure 8. (Color online) Relative change of peak position R of the Gaussian describing the distribution of La-La interatomic bond lengths in the first coordination sphere during heating between 320 and 490 K at different heating rates. Arrows indicate the onsets of the relaxation T_r, glass transition T_g and crystallization T_x temperatures. For purposes of better clarity all curves are vertically offset by 0.003.

reciprocal space analysis (see Figure 7) reveals a monotonous volume expansion between T_g and T_x whereas the La-La bond length shows a more complicated non-monotonous expansion behavior within the same temperature range. Similar trends are observed for runs performed at heating rates 5, 10 and 20 K/min. It should be noted here that the increasing heating rate blurs the observed features and shifts the thermal expansion curves towards higher temperatures. An obvious kinetic behavior can be observed.

As can be seen from Table 1 the transition temperatures such as T_r, T_g and T_x increase as the heating rate Φ increases. Activation energies of the corresponding transitions were calculated according the method proposed by Khonik *et al.* [23]. Based

Table 1. Relaxation temperature T_r, glass transition temperature T_g and crystallization temperature T_x were at different heating rates Φ.

Φ (K/min)	T_r(K)	T_g(K)	T_x(K)
2	373	405	457
5	378	413	470
10	387	421	477
20	394	424	485
50	398	433	499
100	410	444	511

on the extensive literature review they showed that the Kissinger method may lead to false values of the activation energies. They proposed the following linear relation

$$E_a = A(\nu, \Phi)T_a, \tag{7}$$

between the activation energy E_a and the onset temperature T_a, associated with the structural transformation (crystallization). The $A(\nu, \Phi)$ is a function of the apparent attempt frequency ν and the heating rate Φ. Within 18 % accuracy the A value is independent of the apparent attempt frequency if taken in the range $10^{10} \leq \nu \leq 10^{16}$ s^{-1}, wide enough to cover many frequencies reported for structural relaxation of metallic glasses. The dependence of A on the heating rate Φ was established as $A(\Phi) = 2.92 \times 10^{-3} - 1.92 \times 10^{-4} \log \Phi$ in which Φ is taken in K/s [23]. Activation energies of relaxation, glass transition and crystallization processes calculated according Equation (7) are showing no dependence on a heating rate Φ and within experimental uncertainty remain constat. The average activation energies for relaxation, glass transition and crystallization process are 1.18, 1.28 and 1.47 eV, respectively.

4.3. Temperature-Time-Transformation diagram

In order to erase the sample history we remelted it two times by heating up to 823 K and cooling down to room temperature. From the measurement of the thermal expansion in the molten state (not shown here) we see that thermal cycling in this temperature range is a fully reversible process [24]. Therefore one can use a single piece of sample for the determination of the Temperature-Time-Transformation (TTT) diagram. The experiment starts with melting the sample by heating up to 773 K, well above the liquidus temperature (708 K @ 2 K/min). The sample is kept for 1 minute at 773 K just to reach thermal equilibrium. Afterwards we cool the sample with the maximum cooling rate of 120 K/min down to selected temperatures at which we perform isothermal annealing. We wait at the selected temperature until Bragg peaks appear, indicating the initiation of crystallization. This procedure is iterated for many temperatures. It should be noted here that during the whole procedure we instantaneously acquired diffraction patterns with the time resolution of 3 s. Figure 9 shows the obtained

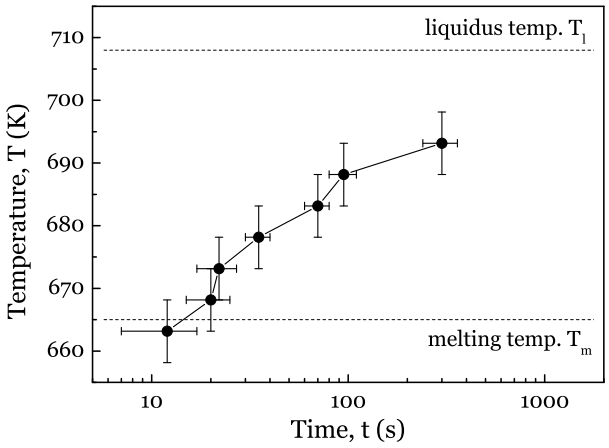

Figure 9. Temperature-Time-Transformation (TTT) diagram for $La_{62}Al_{14}(Cu_{5/6}Ag_{1/6})_{14}Ni_5Co_5$ BMG. Dashed lines indicate melting T_m=665 K and liquidus T_l=708 K temperatures determined at 2 K/min.

TTT diagram. Despite the fact that $La_{62}Al_{14}(Cu_{5/6}Ag_{1/6})_{14}Ni_5Co_5$ bulk metallic glass exhibits rather high glass forming ability, we were not able to observe in-situ formation of BMG upon rapid quenching. The maximum cooling rate (120 K/min) we achieved with the THMS600 heating stage was simply not sufficient to undercool the melt.

5. Conclusions

It has been demonstrated that the analysis of the in-situ XRD constant-rate heating experiments yields thermal expansion data which can be used to monitor subtle changes such as structural relaxation and glass transition, preceding crystallization of the amorphous phase. On varying the heating rate the kinetics of the transitions involved can be observed. Thermal expansion values based on reciprocal space analysis are determined by long range interatomic correlations and show good agreement with conventional dilatometry results performed below the glass transition temperature. XRD is a contact free method, hence measurements above the glass transition T_g are possible. Real space analysis using the reduced pair distribution function $G(r)$ reveals more detailed information about thermal expansion of glassy alloys on the local atomic scale. Our data indicate that reciprocal space analysis based on the principal peak position and real space analysis based on center of the mass of the first coordination shell gives in general different results since they are preferentially sensitive to different correlation lengths.

Acknowledgments

We acknowledge the European Synchrotron Radiation Facility for provision of synchrotron radiation facilities in using beamline ID11. S.M. thanks Deutscher Akademischer Austausch Dienst for providing the DAAD fellowship. Financial supports

from Zhejiang University-Helmholtz cooperation fund, Slovak Ministry of Education (project VEGA 10167/10), the National Natural Science Foundation of China (Grant Nos. 51071141, 50701038, 60776014, 60876002 and 10804096), the Ministry of Education of China (Program for Changjiang Scholars), the Department of Science and Technology of Zhejiang province and Zhejiang University are gratefully acknowledged.

6. References

[1] A. Inoue. *Acta Materialia*, 48:279–306, 2000.
[2] A. Inoue and N. Nishiyama. *Mater. Trans. JIM*, 38:182, 1997.
[3] H. Ma, L.L. Shi, J. Xu, Y. Li, and E. Ma. *Appl. Phys. Lett.*, 87:181915, 2005.
[4] Q.K. Jiang, G.Q. Zhang, L. Yang, X.D. Wang, K. Saksl, H. Franz, R. Wunderlich, H. Fecht, and J.Z. Jiang. *Acta Mater.*, 55:4409, 2007.
[5] Q.K. Jiang, X.D.Wang, X.P. Nie, G.Q. Zhang, H. Ma, H.-J. Fecht, J. Bednarcik, H. Franz, Y.G. Liu, Q.P. Cao, and J.Z. Jiang. *Acta Mater.*, 56:1785, 2008.
[6] T. Egami and S.J.L. Billinge. *Underneath the Bragg Peaks: Structural analysis of complex materials*. Pergamon Press, Elsevier, Oxford, England, 2003.
[7] W. Dmowski, C. Fan, M.L. Morrison, P.K. Liaw, and T. Egami. *Materials Science and Engineering: A*, 471:125–129, 2007.
[8] N. Mattern. *Journal of Non-Crystalline Solids*, 353:1723–1731, 2007.
[9] H.F. Poulsen, J.A. Wert, J. Neuefeind, V. Honkimäki, and M. Daymond. *Nat. Mater.*, 4:33, 2005.
[10] R.T. Ott T.C. Hufnagel and J. Almer. *Phys. Rev. B*, 73:064204, 2006.
[11] X.D. Wang, J. Bednarcik, K. Saksl, H. Franz, Q.P. Cao, and J.Z. Jiang. *Appl. Phys. Lett.*, 91:081913, 2007.
[12] X.D. Wang, J. Bednarcik, H. Franz, H.B. Lou, Z.H. He, Q.P. Cao, and J.Z. Jiang. *Appl. Phys. Lett.*, 94:011911, 2009.
[13] A. Yavari, A. Moulec, A. Inoue, N. Nishiyama, N. Lupu, E. Matsubara, W. Botta, G. Vaughan, M. Michiel, and Å. Kvick. *Acta Mater.*, 53:1611, 2005.
[14] A.P. Hammersley, S.O. Svensson, M. Hanfland, A.N. Fitch, and D. Häusermann. *High Press. Res.*, 14:235, 1996.
[15] Y. Waseda. *The Structure of Non-Crystalline Materials*. McGraw-Hill Inc., 1980.
[16] B. J. Thijsse. *Journal of Applied Crystallography*, 17:61–76, 1984.
[17] T.E. Faber and J.M. Zimman. *Philos. Mag.*, 11:153, 1965.
[18] K. Russew and F. Sommer. *Journal of Non-Crystalline Solids*, 319:289, 2003.
[19] A.I. Taub and F. Spaepen. *Acta Metall.*, 28:1781, 1980.
[20] E. Pineda, I. Hidalgo, P. Bruna, T. Pradell, A. Labrador, and D. Crespo. *Journal of Alloys and Compounds*, 483:578–581, 2009.
[21] D. V. Louzguine-Luzgin, A. Inoue, A. R. Yavari, and G. Vaughan. *Appl. Phys. Lett.*, 88:121926 (3pp), 2006.
[22] D. V. Louzguine-Luzgin and A. Inoue. *Physica B*, 388:290–293, 2007.
[23] V. A. Khonik, K. Kitagawa, and H. Morii. *Journal of Applied Physics*, 87(12):8440–8443, 2000.
[24] J. Bednarcik, C. Curfs, M. Sikorski, H. Franz, and J. Z. Jiang. *Journal of Alloys and Compounds*, 504S:S155–S158, 2010.